Available online at www.sciencedirect.com
ScienceDirect
International Journal of Heat and Mass Transfer 50 (2007) 4105–4116
International Journal of HEAT and MASS TRANSFER
www.elsevier.com/locate/ijhmt

Surface wettability change during pool boiling of nanofluids and its effect on critical heat flux

S.J. Kim [a], I.C. Bang [a], J. Buongiorno [a,*], L.W. Hu [b]

[a] Nuclear Science and Engineering Department, Massachusetts Institute of Technology, 77 Massachusetts Avenue, Cambridge, MA 02139-4307, USA
[b] Nuclear Reactor Laboratory, Massachusetts Institute of Technology, Cambridge, MA, USA

Received 1 September 2006; received in revised form 22 January 2007
Available online 26 March 2007

Abstract

The pool boiling characteristics of dilute dispersions of alumina, zirconia and silica nanoparticles in water were studied. Consistently with other nanofluid studies, it was found that a significant enhancement in critical heat flux (CHF) can be achieved at modest nanoparticle concentrations (<0.1% by volume). Buildup of a porous layer of nanoparticles on the heater surface occurred during nucleate boiling. This layer significantly improves the surface wettability, as shown by a reduction of the static contact angle on the nanofluid-boiled surfaces compared with the pure-water-boiled surfaces. A review of the prevalent CHF theories has established the nexus between CHF enhancement and surface wettability changes caused by nanoparticle deposition. This represents a first important step towards identification of a plausible mechanism for boiling CHF enhancement in nanofluids.

Keywords: Nanofluids; Nanoparticle deposition; Critical heat flux; Pool boiling; Wettability; Contact angle

1. Introduction

Many important industrial applications rely on nucleate boiling, to remove high heat fluxes from a heated surface. These include cooling of high-power electronics, nuclear reactors, chemical reactors and refrigeration systems, to mention a few. Nucleate boiling is a very effective heat transfer mechanism, however it is well known that there exists a critical value of the heat flux at which nucleate boiling transitions to film boiling, a very poor heat transfer mechanism. In most practical applications it is imperative to maintain the operating heat flux below such critical value, which is called the critical heat flux (CHF). Obviously, a high value of the CHF is desirable, because, everything else being the same, the allowable power density that can be handled by a cooling system based on nucleate boiling is roughly proportional to the CHF. Therefore, an increase of the CHF can result in more compact and efficient cooling systems for electronic devices, nuclear and chemical reactors, air conditioning, etc., with significant economic benefits in all these applications.

Addition of solid nanoparticles to common fluids such as water and refrigerants is an effective way to increase the CHF. The resulting colloidal suspensions are known in the literature as nanofluids [1]. Materials used for nanoparticles include chemically stable metals (e.g., gold, silver, copper), metal oxides (e.g., alumina, zirconia, silica, titania) and carbon in various forms (e.g., diamond, graphite, carbon nanotubes, fullerene). Nanoparticles are relatively close in size to the molecules of the base fluid, and thus, if properly prepared, can realize very stable suspensions with little erosion and gravitational deposition over long periods of time. As such, nanofluids lend themselves well to 'real world' applications, contrary to the milli- and microsize particle slurries explored in the past, which quickly settle and often clog the flow channels. At MIT we are conducting research to assess the feasibility of water-based nanofluids for nuclear applications [2].

* Corresponding author. Tel.: +1 617 253 7316; fax: +1 617 258 8863.
E-mail address: jacopo@mit.edu (J. Buongiorno).

0017-9310/$ - see front matter © 2007 Elsevier Ltd. All rights reserved.
doi:10.1016/j.ijheatmasstransfer.2007.02.002

Nomenclature

c	specific heat, J/kg K
D	diameter, m
f	frequency, Hz
g	acceleration of gravity, m/s^2
h	specific enthalpy, J/kg
I	current, A
j	superficial velocity, m/s
k	thermal conductivity, W/m K
L	wire length, m
n''	nucleation site density, m^{-2}
N	microcavity density, m^{-2}
q''	heat flux, W/m^2
r	roughness factor
r	radius, m
$\Re$	radius of curvature, m
S	thermal activity, J/(m K s$^{1/2}$)
T	temperature, °C
V	voltage, V

Greek symbols

δ	thickness, m
$\dot{\delta}$	growth rate, m/s
$\Delta\tau$	time, s
γ	surface energy, N/m
φ	nanoparticle volumetric fraction
κ	constant
θ	contact angle, degree or rad
ρ	density, kg/m^3
σ	surface tension, N/m
τ	time, s

Subscripts

b	bubble
c	cavity
cr	critical
d	bubble departure
d	macrolayer dryout
e	equivalent
f	liquid phase
fg	liquid-to-vapor transition
g	vapor phase
h	hovering, heater
m	microlayer
p	nanoparticle
sat	saturation
SL	solid–liquid
SV	solid–vapor
w	wall, bubble wait

As of today (7/06), over 10 studies of CHF and nucleate boiling in nanofluids have been reported in the literature [3–14]. The findings can be summarized as follows:

- Significant CHF enhancement (up to 200%) occurs with various nanoparticle materials, including silicon, aluminum and titanium oxides.
- The CHF enhancement occurs at relatively low nanoparticle concentrations, typically less than 1% by volume.
- During nucleate boiling some nanoparticles precipitate on the surface and form a layer whose morphology depends on the nanoparticle materials.
- Some studies report no change of heat transfer in the nucleate boiling regime [3,5], some report heat transfer deterioration [4,9] and others heat transfer enhancement [6,11].

Researchers have carefully reported the experimental data, but they have made few attempts at and little progress in explaining the CHF enhancement mechanism. The main objective of this paper is to start developing an insight of the CHF enhancement mechanism in nanofluids. The structure of the paper is as follows. Preparation and characterization of our nanofluids is reviewed in Section 2. New CHF and surface wettability data are presented in Section 3. The data are discussed in light of the CHF theories in Section 4. The conclusions are provided in Section 5.

2. Preparation and characterization of nanofluids

We have selected three nanoparticle materials for this study, i.e., alumina (Al_2O_3), zirconia (ZrO_2) and silica (SiO_2). Water-based nanofluids of these three materials were purchased from Sigma–Aldrich (alumina and zirconia) and Applied Nanoworks (silica). The vendor-specified concentration of the nanofluids was 10% by weight, which we verified with thermo-gravitometric analyses. The as-purchased nanofluids were then diluted with deionized water to the low concentrations of interest for the CHF experiments, i.e., 0.001%, 0.01% and 0.1% by volume. The size (effective diameter) of the nanoparticles in the dilute nanofluids was measured with the dynamic light scattering technique and ranged from 110 to 210 nm for alumina nanofluids, 110 to 250 nm for zirconia nanofluids, and 20 to 40 nm for silica nanofluids. An important parameter for the colloidal stability of oxide nanoparticles is pH, which determines the electrostatic charge on the particles surface. To prevent the particles from agglomerating and settling, the pH has to be far from the so-called iso-electric point (IEP), i.e., the pH at which there exists an equal number of positively and negatively charged particles in the colloid. Values of the pH for our dilute alumina, zirconia and silica nanofluids were measured to be 4–5, 3–5 and 7–10, respectively, which are far from the IEP of alumina (~9), zirconia (~8) and silica (~3). All nanofluids used in our experiments were found to be colloidally stable (i.e., did

not sediment) at the reported nanoparticle concentrations in the reported pH ranges, with no surfactant addition.

Various parameters relevant to two-phase heat transfer were also measured or estimated. First, the boiling point of the dilute nanofluids was measured with a thermocouple and found to be within ±1 °C of pure water. The surface tension, thermal conductivity and viscosity of the nanofluids were measured by means of a Sigma 703 tensiometer, a KD2 thermal conductivity probe and a capillary viscometer, respectively. These properties were found to differ negligibly from those of pure water, as shown in Figs. 1–3. The nanofluid density can be calculated as $\rho_p\varphi + \rho_f(1-\varphi)$, where φ is the nanoparticle volumetric fraction, and ρ_p and ρ_f are the density of the nanoparticle material and base fluid, respectively. For example, for $\varphi \sim 0.1\%$v, $\rho_p \sim 4$ g/cm^3 and $\rho_f \sim 1$ g/cm^3 the deviation from pure water is expected to be only 0.3%. Assuming that the nanoparticles are as volatile as the water molecules, the density of the nanofluid vapor can be calculated as $\rho_g[\rho_p\varphi + \rho_f(1-\varphi)]/[\rho_g\varphi + \rho_f(1-\varphi)]$, which gives deviations from the pure water vapor density of the order of 0.4% at the conditions of interest. In reality the deviation will be even smaller because the nanoparticles are less volatile than the water molecules. Finally, the low nanoparticle concentration and the absence of chemical reactions between the nanoparticles and water suggest that the heat of vaporization should not change either. In summary, the transport and thermodynamic properties of our dilute nanofluids are very similar to those of pure water.

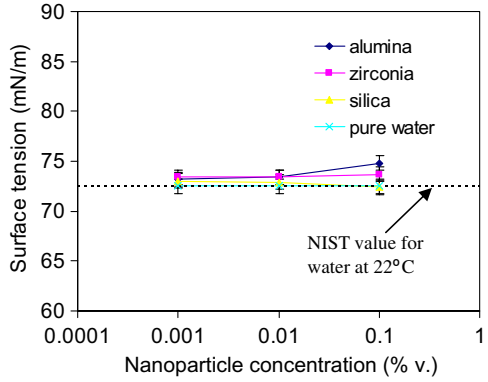

Fig. 1. Surface tension of nanofluids at room temperature.

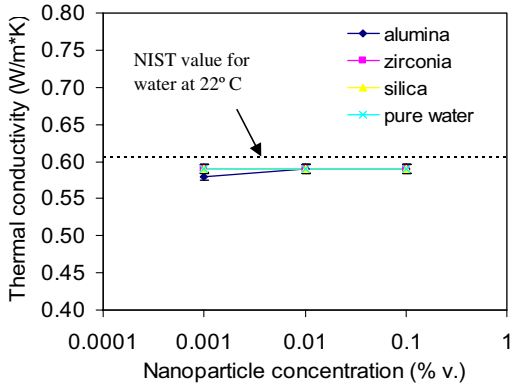

Fig. 2. Thermal conductivity of nanofluids at room temperature.

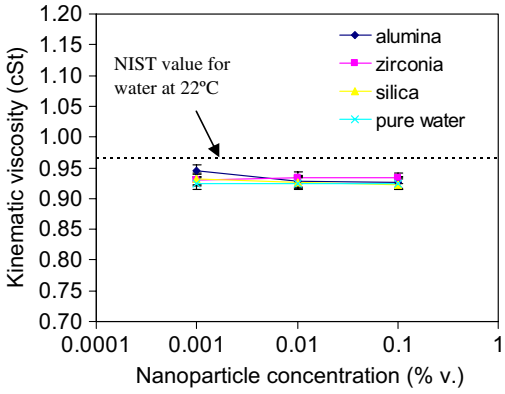

Fig. 3. Kinematic viscosity of nanofluids at room temperature.

3. Experimental

3.1. CHF experiments with wires

The CHF of deionized pure water and nanofluids was measured in the apparatus shown in Fig. 4, which basically consists of a wire heater horizontally submerged in the test fluid at atmospheric pressure, surrounded by an isothermal bath. The wire, made of stainless steel grade 316, has a 0.381-mm diameter and 12-cm length. The wire is soft soldered with a silver–lead solder to the copper electrodes and heated by resistance heating with a DC power supply of 20-V and 120-A capacity. Voltage and current are measured with a Keithley and Hewlett–Packard multimeters. The wire temperature is estimated from measurement of the electric resistance and using the known resistivity–temperature curve for stainless steel. The fluid bulk temperature is measured with a K-type thermocouple (nominal uncertainty ±1.1 °C, as specified by the manufacturer). The experimental procedure is as follows. First, the isothermal bath and the test fluids are taken to the desired temperature by the preheaters. The wire is heated up at low heat flux to remove any incondensable gas bubbles sticking to the surface. After the gas is removed, the power is increased in small steps of ~0.2 V until CHF occurs. CHF is detected visually (i.e., the wire glows) and/or electrically (i.e., the electric resistance suddenly increases), thus terminating the experiment. Heat fluxes are calculated from the following equation:

$$q'' = \frac{IV}{\pi LD} \tag{1}$$

The uncertainties on the current, voltage, heated length and wire diameter values are less than 3%, 4%, 3% and 1%, respectively, resulting in an uncertainty of less than 6% on the heat flux.

Measured CHF values are shown in Fig. 5. Significant CHF enhancement is observed for all nanofluids, up to

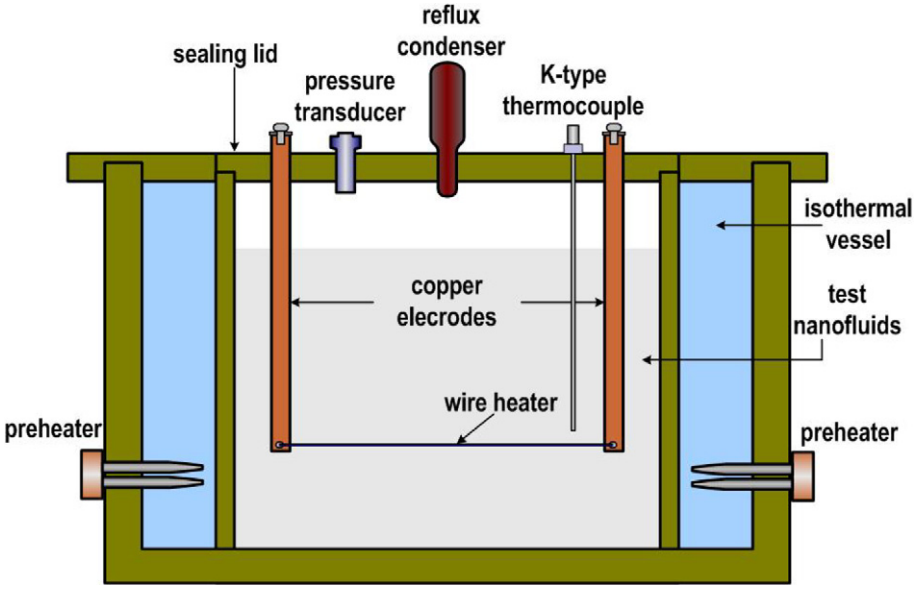

Fig. 4. Resistance heating wire pool boiling facility.

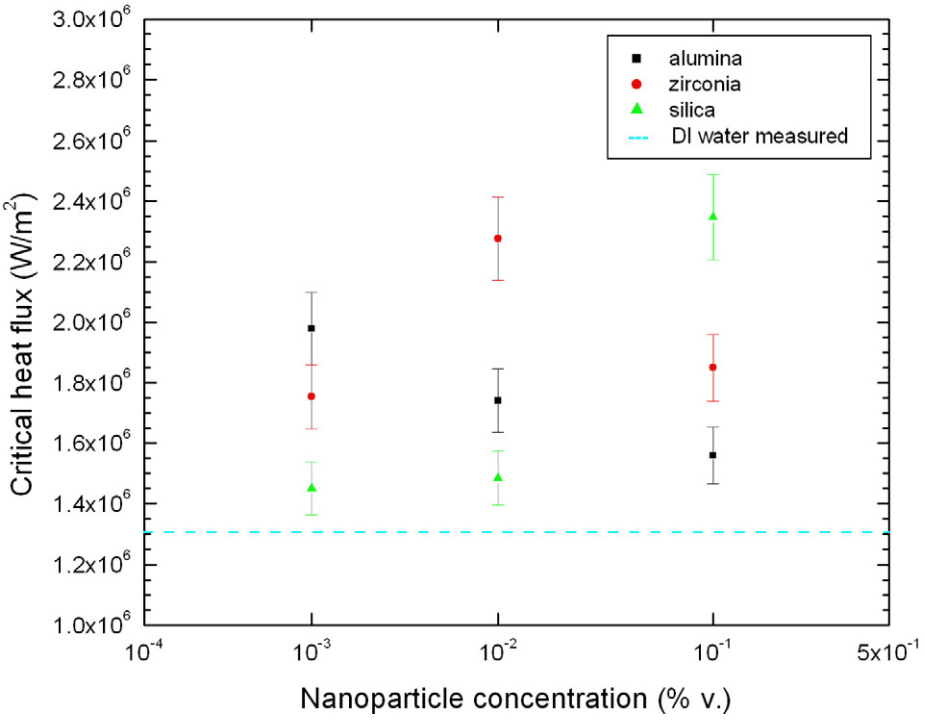

Fig. 5. CHF data for pure water and alumina, zirconia and silica nanofluids.

52% with alumina nanofluids, up to 75% with zirconia nanofluids and up to 80% for silica nanofluids. The CHF dependence on nanoparticle concentration is a bit erratic, but not unprecedented for nanofluids [9]. The boiling regimes of pure water and a nanofluid are compared in Fig. 6. At the low heat flux (Fig. 6a and b), both fluids are in the nucleate boiling regime. At the high heat flux, pure water has exceeded CHF and thus a stable vapor film blankets the wire (film boiling), which is glowing red (Fig. 6c). However, the nanofluid (Fig. 6d) is still well within the nucleate boiling regime.

Typical boiling curves for pure water and two nanofluids are shown in Fig. 7. Note that the nanofluids have higher CHF, but lower nucleate boiling heat transfer coefficient. The deterioration of nucleate boiling suggests that a surface effect may be at work. Scanning electron microscope (SEM) analysis of the wire surface reveals that the surface is clean during pure water boiling (Fig. 8a), but a

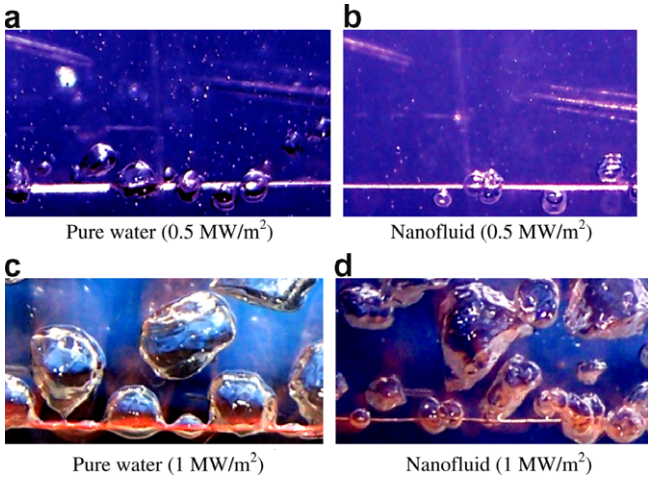

Fig. 6. Pool boiling of pure water and 0.01%v alumina nanofluid at the same heat flux on stainless steel wire.

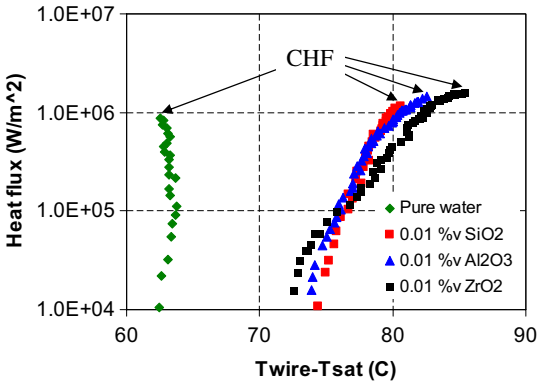

Fig. 7. Boiling curves for stainless steel wire. Uncertainties in the slope of the resistivity–temperature curve for stainless steel and the non-negligible temperature drop within the wire contribute to the unusually high values of the superheat in this boiling curve.

porous layer builds up during nanofluid boiling (Fig. 8b). We believe this layer is due to nanoparticle precipitation caused by nucleate boiling, as explained in Section 4.1

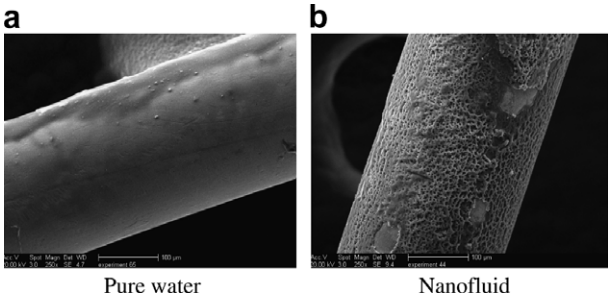

Fig. 8. SEM images of steel wires taken after boiling pure water and 0.01%v alumina nanofluid.

below. Energy dispersive spectrometer (EDS) analysis of the layer confirms that it is made of nanoparticle material. The presence of a porous layer on the surface undoubtedly has an impact on boiling heat transfer through changes in surface area, roughness and wettability, as explained in the following sections.

3.2. Flat heater experiments

Use of a thin wire heater is convenient for CHF experiments, but its high curvature makes it inconvenient for surface analysis, such as required to study the porous layer. For this purpose we switched to flat plates, 5 mm wide, 45 mm long, 0.05 mm thick, made of stainless steel grade 316 (Fig. 9). Using the apparatus of Fig. 4, several flat heaters were boiled in nanofluids for a period of 5 min and at a heat flux of 500 kW/m^2. A new (clean) heater was used for each experimental run. The SEM and EDS analyses again revealed that some nanoparticles precipitate on the heater surface and form irregular porous structures, which do not appear during boiling of pure water (Fig. 10).

The porous layer was analyzed more quantitatively with a Tencor P-10 surface profilometer, which gave the images shown in Fig. 11. The surface boiled in pure water is very smooth, while the surface boiled in the nanofluid presents irregular peak-and-valley structures, which are consistent

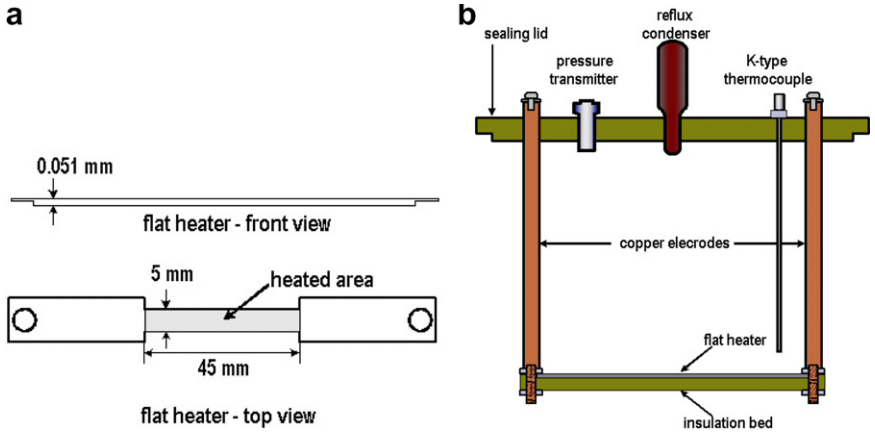

Fig. 9. (a) Flat heater, (b) heater assembly.

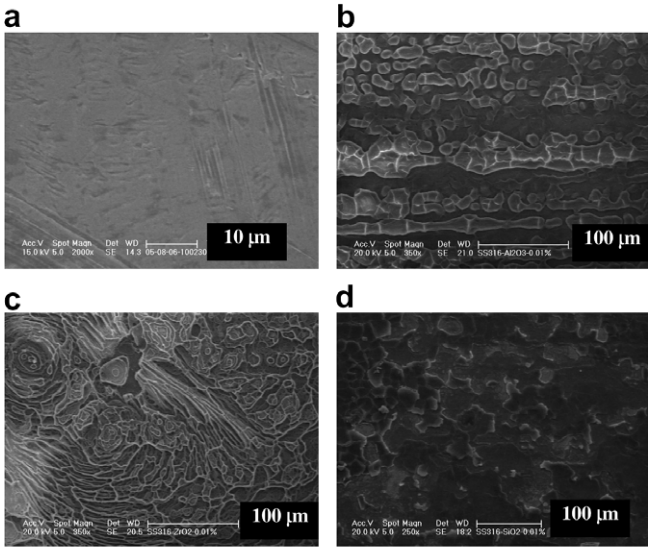

Fig. 10. SEM images of flat heater surface boiled in (a) pure water, (b) 0.01%v alumina nanofluid, (c) 0.01%v zirconia nanofluid, (d) 0.01%v silica nanofluid.

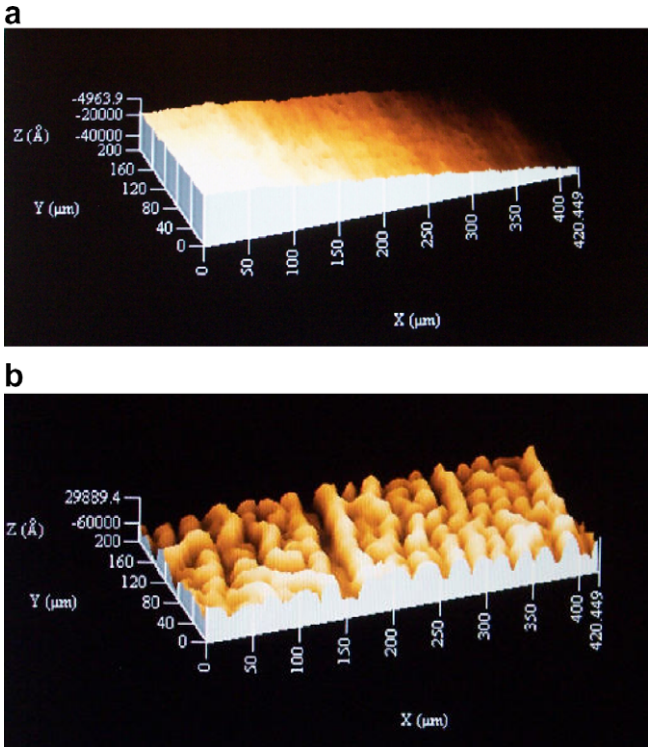

Fig. 11. Profilometer images of the flat heater surface after boiling (a) pure water and (b) 0.01%v alumina nanofluid. The rms roughness values are ~0.1 and ~2 μm, respectively. Similar results were obtained with the other nanofluids.

with the SEM images of Figs. 8 and 10. The roughness and total area of the surface boiled in nanofluid are about twenty times and five times higher than those of the surface boiled in pure water, respectively.

Another important effect caused by the porous layer is the increase in surface wettability. The static contact angle, θ, was measured for sessile droplets of pure water and nanofluids at 22 °C in air on the clean and nanoparticle-fouled surfaces boiled in nanofluids. The uncertainty on such measurements is estimated to be $\pm 10°$. Low values of the contact angle correspond to high surface wettability. A few representative cases are shown in Fig. 12. The complete contact angle database is reported in Table 1. A rather dramatic decrease of the contact angle on the fouled surfaces is evident. Such decrease occurs with pure water as well as nanofluid droplets, thus suggesting that wettability is enhanced by the porous layer on the surface, not the nanoparticles in the fluid. In another research, Wasan and Nikolov [15] found that ordering of nanoparticles near the liquid/solid contact line can improve the spreading of nanofluids.

4. Data interpretation

The experiments presented in Section 3 have shown that nanofluids exhibit enhanced CHF at low nanoparticle concentrations, that during nanofluid boiling the heater surface becomes coated with a porous layer of nanoparticles, and that such layer significantly increases surface wettability. In this section we address some key questions related to the above observations. Why do nanoparticles deposit on the surface during nucleate boiling? Why does the nanoparticle layer enhance wettability? What effect does the nanoparticle layer have on nucleate boiling and CHF?

4.1. Why the nanoparticles deposit on the surface during nucleate boiling?

We have observed no significant deposition of nanoparticles while handling nanofluids or measuring their properties or even in single-phase convective heat transfer experiments, which are being run in our lab. Thus, we concluded that development of the nanoparticle layer shown in Figs. 8, 10 and 11 is a direct consequence of boiling, but what is the mechanism of nanoparticle deposition on the surface during nucleate boiling? It is well known that a thin liquid microlayer develops underneath a vapor bubble growing at a solid surface [16]. Microlayer evaporation with subsequent settlement of the nanoparticles initially contained in it could be the reason for the formation of the porous layer. To verify the plausibility of this hypothesis, we make use of the following simple model. The volume of nanoparticles contained in the liquid microlayer is $\delta_m \frac{\pi}{4} D_b^2 \varphi$, where δ_m is the thickness of the microlayer and D_b is the bubble departure diameter. The number of bubbles generated per unit time and surface area is $n'' f_b$, where n'' is the active nucleation site density and f_b is the bubble departure frequency. Then the rate of growth of the nanoparticle layer on the surface, $\dot{\delta}$, is

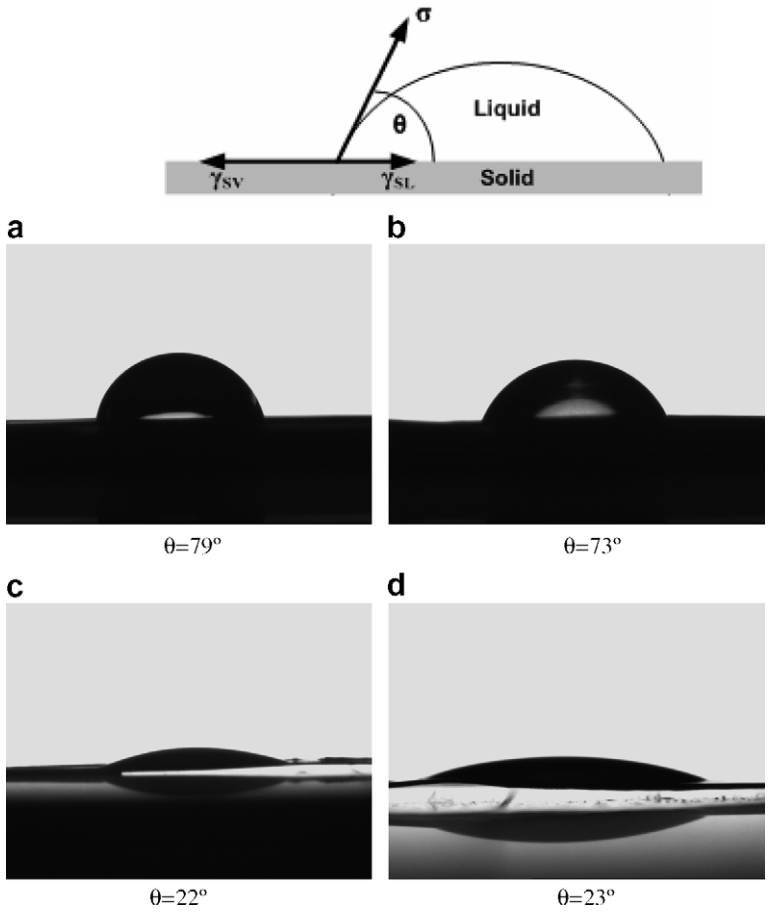

Fig. 12. Static contact angles of 5-μL sessile droplets on stainless steel surfaces, measured with a Krüss goniometer equipped with a camera monitor. (a) Pure water droplet on surface boiled in pure water, (b) 0.01%v alumina nanofluid droplet on surface boiled in pure water, (c) pure water droplet on surface boiled in 0.01%v alumina nanofluid, (d) 0.01%v alumina nanofluid droplet on surface boiled in 0.01%v alumina nanofluid.

Table 1
Static contact angles for water and nanofluids on clean and fouled surfaces

Fluid	Pure water	Al_2O_3 nanofluid			ZrO_2 nanofluid			SiO_2 nanofluid		
Nanoparticle concentration (%v)	0	0.001	0.01	0.1	0.001	0.01	0.1	0.001	0.01	0.1
Clean surface	79°	80°	73°	71°	80°	80°	79°	71°	80°	75°
Nanofluid boiled surface	8–36°[a]	14°	23°	40°	43°	26°	30°	11°	15°	21°

[a] 22–30° on surfaces boiled in alumina nanofluids, 16–36° on surfaces boiled in zirconia nanofluids, 8–18° on surfaces boiled in silica nanofluids.

$$\dot{\delta} \sim \delta_m \frac{\pi}{4} D_b^2 \varphi n'' f_b \tag{2}$$

The active nucleation site density can be estimated from the energy balance at the surface as $n'' \sim q''/\left(\frac{\pi}{6} D_b^3 \rho_g h_{fg} f_b\right)$, where q'' is the heat flux (500 kW/m^2 in our case). Substituting this expression into Eq. (2), we get

$$\dot{\delta} \sim \frac{3}{2} \frac{\delta_m \varphi q''}{D_b \rho_g h_{fg}} \tag{3}$$

The bubble departure diameter for water at atmospheric pressure can be estimated from the Cole and Rosenhow's correlation [17], which gives $D_b \sim 2.4$ mm. Assuming also $\delta_m \sim 1$ μm, as recommended by Collier and Thome [16] for water at atmospheric pressure, we find $\dot{\delta} \sim 0.02$ μm/s for $\varphi = 10^{-4}$. The duration of the experiments with the flat heaters is approximately 5 min, resulting in a thickness of the nanoparticle layer of about 6 μm, which is the same order of magnitude of the structures observed with the SEM and profilometer. Given the uncertainties in the model parameters (especially the values of D_b and δ_m), the agreement is deemed acceptable.

Mechanisms of nanoparticle diffusion to the surface (such as Brownian motion or thermophoresis) were neglected in the previous discussion. This is a good assumption, as nanoparticle transport is dominated by the vigorous mixing caused by bubble nucleation, growth and departure. In other words, the nanoparticles are trans-

ported by the fluid over distances of millimeters every 10–30 ms (i.e., the typical bubble cycle time), while over the same period of time diffusion mechanisms can transport them at most a few microns.

4.2. Why the nanoparticle layer enhances surface wettability

To understand the enhancement of wettability, we consider Young's equation

$$\cos\theta = \frac{\gamma_{SV} - \gamma_{SL}}{\sigma} \tag{4}$$

which relates the static contact angle to the surface tension, σ, and the so-called adhesion tension, $\gamma_{SV} - \gamma_{SL}$. The adhesion tension of water on clean steel is ~10 mN/m and its surface tension is ~72 mN/m, so Young's equation yields a contact angle of about 82°, which is in good agreement with the measured angle (Fig. 12a). If the surface is not smooth, the effective solid–liquid contact area differs from the smooth contact area. Wenzel [18] defines a roughness factor, r, as the ratio of the effective contact area to the smooth contact area. The free energy of the solid–liquid interface on a rough surface is then r times the free energy of a perfectly smooth surface with the same apparent contact area. Therefore, Young's equation needs to be modified as follows [18]:

$$\cos\theta = \frac{\gamma_{SV} - \gamma_{SL}}{\sigma} r \tag{5}$$

Eq. (5) suggests that the contact angle on a rough surface depends on three parameters, i.e., the surface tension, the adhesion tension and the roughness factor. The surface tension of our nanofluids was found to minimally differ from that of pure water (Fig. 1). On the other hand the adhesion tension of water increases significantly in going from a clean metal to an oxide, e.g., from ~10 mN/m (stainless steel) to ~60 mN/m (alumina). Such change in adhesion tension alone reduces the contact angle to ~34°, as calculated from Eq. (5) assuming $r = 1$. This is consistent with other studies showing that surface oxidation decreases the contact angle [19]. The porous layer also increases the effective contact area. Thus the roughness factor, r, is greater than unity, which also contributes to the contact angle reduction in our case. To evaluate r, we can use the information obtained with the profilometer. For the situation of Fig. 11 the estimated surface areas are about 84,000 μm^2 (clean surface) and 470,000 μm^2 (nanoparticle-fouled surface), resulting in $r \sim 5.6$. For $r \sim 5.6$ the contact angle decreases to ~39°, as calculated from Eq. (5) with nominal adhesion tension (~10 mN/m) and surface tension (~72 mN/m). In summary, a simple analysis of the modified Young's equation suggests that the enhancement in wettability (decrease in contact angle) is caused by a combination of two effects, i.e., an increase of adhesion tension and an increase of surface roughness. Both effects are at work and large enough to cause a pronounced reduction of the contact angle.

4.3. Effect of nanoparticles on nucleate boiling

The most remarkable characteristic of nucleate boiling in our nanofluid experiments was the reduction of the heat transfer coefficient, as revealed by the boiling curve shift to the right (Fig. 7). A possible reason for this shift is the buildup of the nanoparticle layer, which creates a resistance to heat transfer from the heater (metal) surface to the fluid. The estimated temperature drop can be up to 10 °C for oxide layers of 1–10 μm, assuming an arbitrary layer porosity of 50% and a heat flux of the order of 1 MW/m^2. Incidentally, we note that the effect of the nanoparticle layer on the heater electric resistance is negligible because alumina, zirconia and silica have electrical conductivities many orders of magnitude lower than steel.

Another reason for the boiling curve shift could be the reduction of nucleation site density caused by the decrease in contact angle. Wang and Dhir [19] correlated their experimental data to find the following expression for the nucleation site density:

$$n'' \propto N_c(1 - \cos\theta)(T_w - T_{sat})^6 \tag{6}$$

where N_c is the number of microcavities per unit surface area and $T_w - T_{sat}$ is the wall superheat. According to Eq. (6) a decrease of the contact angle would tend to decrease the active nucleation site density and thus the heat transfer coefficient. However, this effect could be countered by the higher number of microcavities (N_c), which the porous layer likely creates. Lacking direct measurement of the nucleation site density, the link between boiling curve shift and nanoparticle layer cannot be conclusively elucidated. It is interesting to note that heat transfer *deterioration* in the nucleate boiling regime was also observed by Das et al. [4] and Bang and Chang [9]. On the other hand, heat transfer *enhancement* was reported by Dinh et al. 6] and Wen and Ding [11], while You et al. [3] and Vassallo et al. [5] reported *no change* of heat transfer in the nucleate boiling regime at all. Wen and Ding [11] proposed that these conflicting trends could be due to poorly characterized/reported factors such as initial surface roughness, presence of surfactants, agglomeration of particles, surface contamination, etc. However, this is an area that clearly warrants additional study.

4.4. Effect of nanoparticles on CHF

The nanofluid literature is generally deficient in explaining the CHF enhancement mechanism in nanofluids. In all honesty this is no easy task. Despite several decades of intense study a consensus explanation of the physical mechanism causing CHF, or departure from nucleate boiling (DNB), is yet to be found, even for the simple situation of a pure fluid, let alone nanofluids. A plethora of hypotheses has been formulated, most of which generally fall into one of the following four categories:

- Hydrodynamic instability theory
- Macrolayer dryout theory
- Hot/dry spot theory
- Bubble interaction theory

We shall now interrogate these DNB theories with respect to their ability to explain the CHF gains obtained with nanofluids. The main objective of the following discussion is not to recommend a correlation to calculate nanofluid CHF, but to determine if the DNB theories support the link between an increase in surface wettability and CHF enhancement.

4.4.1. Hydrodynamic instability theory

The hydrodynamic instability theory assumes that the occurrence of DNB is dominated by the hydrodynamics of the countercurrent flow of vapor and liquid far above the heated surface [20,21]. Specifically, it is postulated that at DNB the downflow of fresh liquid to the heated surface is prevented by the rising vapor.

The superficial vapor velocity, j_g, leading to the onset of instability above a flat upward-facing heated surface is given by the following equation [21]:

$$j_g = 0.13\left[\frac{\sigma(\rho_f-\rho_g)g}{\rho_g^2}\right]^{1/4} \tag{7}$$

Thus the CHF (for saturated boiling) can be calculated simply as

$$q''_{cr} = \rho_g j_g h_{fg} \tag{8}$$

For thin cylindrical heaters of diameter D, Eq. (8) has to be modified as follows [16]:

$$q''_{cr} = 1.12\frac{\rho_g j_g h_{fg}}{\left[D\Big/\sqrt{\frac{\sigma}{g(\rho_f-\rho_g)}}\right]^{1/4}} \tag{9}$$

Eq. (9) suggests that, for a given heater, CHF depends only on the fluid properties. However, the nanofluid properties are very close to those of pure water, as explained in Section 2, so Eq. (9) would predict no CHF enhancement in nanofluids. Because of its inability to account for surface effects (i.e., roughness, wettability), the hydrodynamic instability theory must be discarded as an interpretative tool for nanofluid CHF. In fact in recent years the hydrodynamic theory has been openly questioned also for pure fluids [6].

4.4.2. Macrolayer dryout theory

In this approach it is assumed that large mushroom-shaped bubbles (fed by many individual nucleation events) hover above the heated surface for a relatively long time before departing. These bubbles are separated from the surface by a liquid macrolayer, the word "macro" marking the distinction from the microlayer forming underneath an individual bubble as it grows out of a nucleation site (see Section 4.1 above). The assumption is that DNB occurs if the macrolayer dries out during a hovering cycle [22,23].

To estimate the impact of the observed contact angle change on the macrolayer, we can use Sadasivan et al.'s model [23]. This model postulates that bubbles growing at neighboring active cavities can coalesce laterally at a certain stage during the growth phase, before they depart from the surface. According to the model the macrolayer is the volume of liquid trapped between the vapor bubbles below the plane of coalescence (Fig. 13a). The bubbles are assumed to have uniform size with radius r_b, and be uniformly distributed over the heater surface. Therefore, for a $2r_b \times 2r_b$ unit cell the volume of liquid trapped below the plane of coalescence is $4r_b^3\cos\theta - \left[\frac{1}{3}\pi r_b^3(3\cos\theta - \cos^3\theta)\right]$. The equivalent thickness of the macrolayer, δ_e, is then calculated assuming uniform spreading of the trapped liquid over the surface

$$\delta_e = r_b\left[\cos\theta - \frac{\pi}{12}(3\cos\theta - \cos^3\theta)\right] \tag{10}$$

For given r_b, the macrolayer thickness increases with decreasing contact angle (Fig. 13b). The time to dry out the macrolayer, τ_d, can be estimated from the energy balance at the surface

$$\tau_d = \frac{\delta_e \rho_f h_{fg}}{q''} \tag{11}$$

Sadasivan et al.'s hypothesize that DNB occurs if $\tau_d < \tau_h$, where τ_h is the hovering time of the mushroom bubble. Since τ_h depends mostly on hydrodynamics and only weakly on the heat flux [24], the increase in τ_d has a direct effect on CHF, i.e., the value of the heat flux at which DNB occurs is roughly proportional to τ_d. Eq. (10) suggests that a contact angle reduction from, say, 70° to 20° would

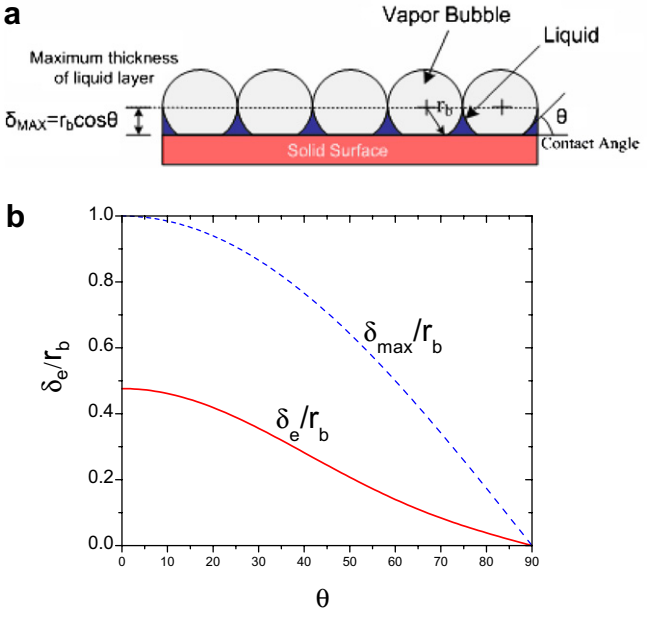

Fig. 13. (a) Sadasivan et al.'s [23] macrolayer concept. (b) Macrolayer thickness vs contact angle.

increase the liquid layer thickness about 4-fold, which results in a 4-fold increase of the dryout time, and thus in roughly a 4-fold increase of the CHF. Recognizing that the CHF enhancement measured in our experiments was not quite so large, we can however conclude that the macrolayer dryout theory points to a strong correlation between CHF enhancement and increase in surface wettability caused by nanoparticle deposition.

4.4.3. Hot/dry spot theory

If the heat flux is high, hot/dry spots develop within the bases of the bubbles growing at certain nucleation sites. The hot/dry spots can be reversible or irreversible. They are reversible if rewetting occurs upon bubble departure. They are irreversible if rewetting does not occur, which causes a runaway excursion of the surface temperature and eventually burnout [25]. In principle the presence of the nanoparticle layer on the surface can help delay DNB in two ways. First, the layer may assist in dissipating the hot spot by enhancing radial conduction on the surface. Second, its increased wettability promotes rewetting upon bubble departure.

The first effect is small. Heat conduction within the heater, radially from a hot/dry spot to the surrounding cooler areas, can promote dissipation of the hot/dry spot. The effect of conduction in the heater is typically described by the so-called 'thermal activity', S:

$$S = D\sqrt{\rho_h c_h k_h} \tag{12}$$

which is the product of the heater characteristic dimension (D) and the heater material effusivity $\left(\sqrt{\rho_h c_h k_h}\right)$. The effusivity of the materials of interest to this study is reported in Table 2. The higher the thermal activity, the more effectively conduction can dissipate the hot/dry spot. According to Arik and Bar-Cohen [26] the effect 'saturates' for $S > 8$ J/(m K s$^{1/2}$). The value of the thermal activity for our stainless steel wire is about 1.8 J/(m K s$^{1/2}$), suggesting that rewetting may be conduction limited. Precipitation of a high-effusivity nanoparticle layer on the surface of the wire increases the heater thermal activity and thus can delay DNB. However, the thickness of the nanoparticle layer is of the order of a few microns, thus adding a meager <0.1 J/(m K s$^{1/2}$) to the thermal activity.

To assess the importance of the wettability effect, we can avail ourselves of the model proposed by Theofanous and Dinh [27], who considered the microhydrodynamics of the solid–liquid–vapor line at the boundary of a hot/dry spot.

Table 2
Thermo-physical properties of the heater and nanoparticle materials of interest to this study

	ρ_h (g/cm^3)	c_h (J/kg K)	k_h (W/m K)	$\sqrt{\rho_h c_h k_h}$ (J/(m K s$^{1/2}$))
Steel	8.2	470	13.4	~7200
Al_2O_3	4.0	760	~40	~11,100
ZrO_2	6.0	420	~2	~2200
SiO_2	2.6	745	~8	~3900

They postulate that DNB occurs when the evaporation recoil force, which drives the liquid meniscus to recede, becomes larger than the surface tension force, which drives the meniscus to advance and rewet the hot/dry spot. On this basis, they derived the following expression for the CHF:

$$q''_{cr} = \kappa^{-1/2}\rho_g h_{fg}\left[\frac{\sigma(\rho_f - \rho_g)g}{\rho_g^2}\right]^{1/4} \tag{13}$$

Note that Eqs. (13) and (8) are essentially the same, except for the parameter κ, which is the coefficient of proportionality between the radius of curvature of the liquid meniscus, $\Re$, and the capillary length:

$$\Re = \kappa\sqrt{\frac{\sigma}{g(\rho_f - \rho_g)}} \tag{14}$$

Theofanous and Dinh [27] state that κ is a surface-dependent parameter that "for a well-wetting surface is smaller than for a poorly wetting surface", however they do not provide an analytical expression for it. Using elementary geometry and Lord Rayleigh's formula for the volume of a static liquid meniscus [28], the average radius of curvature of the meniscus can be estimated as

$$\Re = \frac{\sqrt{\frac{\sigma}{g(\rho_f-\rho_g)}}}{\sqrt{1 - \frac{\sin\theta}{2} - \frac{\pi/2-\theta}{2\cos\theta}}} \tag{15}$$

Comparing Eqs. (14) and (15), we can get an expression for κ:

$$\kappa = \left(1 - \frac{\sin\theta}{2} - \frac{\pi/2-\theta}{2\cos\theta}\right)^{-1/2} \tag{16}$$

The values of κ for $\theta \sim 70^\circ$ (clean surface) and $\theta \sim 20^\circ$ (nanoparticle-fouled surface) are about 7.10 and 2.36, respectively, thus Eq. (13) suggests that the CHF would increase by a factor $\sqrt{7.10/2.36} \sim 1.73$, or 73%. This estimate is remarkably close to the CHF enhancement observed in our experiments. In summary, the hot/dry spot theory also seems to corroborate the link between increased surface wettability and CHF enhancement in nanofluids.

4.4.4. Bubble interaction theory

The simplest version of this theory postulates that DNB occurs when at high superheat the bubble number and departure frequency become so high that the bubbles coalesce radially, thus preventing liquid access to the surface [29]. More sophisticated theories include the effect of the shear force generated by the mutual interaction of the growing and departing bubbles [30]. Such shear force cuts the bubble growth cycle prematurely, resulting in a significantly lower bubble departure diameter, and thus in lower latent heat removal upon departure. This effect can become dominant to the point where a further increase of the wall

superheat actually causes a decrease of the heat flux. This slope reversal marks the DNB point on the boiling curve.

Here we use Kolev's model for nucleate boiling [30], which accounts for the effect of shear on bubble growth. The model establishes the following relationship between the heat flux in the nucleate boiling region, q'', and the wall superheat, $T_w - T_{sat}$:

$$q'' \propto \frac{n''^{1/4}(T_w - T_{sat})^2}{\left(1 + 0.3\frac{\Delta\tau_w}{\Delta\tau_d}\right)^{1/2}} \tag{17}$$

where $\Delta\tau_w$ and $\Delta\tau_d$ are the bubble wait time and departure time at the heated surface, respectively. In Eq. (17) we have omitted the dependence on the thermophysical properties of the fluid in light of the discussion in Section 2. The nucleation site density is given by the Wang and Dhir [19] correlation, Eq. (6). As far as $\Delta\tau_w$ and $\Delta\tau_d$ are concerned, the procedure for their calculation is described in detail by Kolev [30], and will not be repeated here. For our purposes it will be sufficient to keep in mind that $\Delta\tau_d$ is a strong function of n'' (and thus of the wall superheat, $T_w - T_{sat}$, via Eq. (6)), in such a way that the ratio $\Delta\tau_w/\Delta\tau_d$ is small at low superheat (in the so-called isolated bubble regime), but rapidly grows and becomes significantly larger than unity as the superheat increases. This behavior is caused by the rapid increase of the nucleation events at the heated surface; such events produce a significant shear force that causes the bubbles to depart at an earlier stage of their growth, i.e., the shear force reduces $\Delta\tau_d$. Because the $\Delta\tau_w/\Delta\tau_d$ ratio is at the denominator of Eq. (17), its large increase at very high superheat causes the slope of the boiling curve to reverse, and it is such reversal that identifies the DNB point (Fig. 14). Therefore, a unique feature of Eq. (17) is its ability to predict the DNB point as a natural evolution of nucleate boiling, without the need for a separate CHF model/correlation.

According to Kolev's model a change of the contact angle θ can have a major effect on CHF, as shown in Fig. 14. In this figure the reference case is $\theta = \pi/2$, to which all other cases have been normalized. CHF increases as the contact angle decreases, and the magnitude of the increase is in the same range of our experimental observations. Therefore, we conclude that the bubble interaction theory also supports the notion of surface wettability improvement as a plausible cause of the CHF enhancement in nanofluids. Interestingly, the bubble interaction theory predicts that CHF enhancement corresponds to deterioration of nucleate boiling heat transfer, which is consistent with our experiments (see Fig. 7).

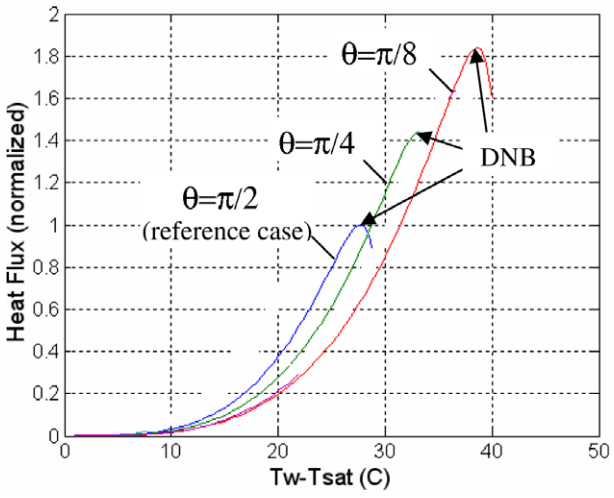

Fig. 14. Effect of contact angle on the boiling curve.

5. Conclusions

The main findings of this study are as follows:

- Dilute dispersions of alumina, zirconia and silica nanoparticles in water exhibit significant CHF enhancement in boiling experiments with wire heaters.
- During nucleate boiling some nanoparticles deposit on the heater surface to form a porous layer.
- This layer improves the wettability of the surface considerably, as measured by a marked reduction of the static contact angle.
- A review of the prevalent CHF theories demonstrates that the higher wettability can produce CHF enhancement which is consistent in magnitude with the experimental observations.

The first two findings are in agreement with other results previously reported in the nanofluid literature. However, we believe this paper makes the first substantial breakthrough in understanding the mechanism of CHF enhancement in nanofluids, by establishing the nexus between CHF and surface wettability changes caused by nanoparticle deposition. To elucidate such mechanism more definitively, additional work is surely needed, including a thorough characterization of the layer growth during boiling and direct measurement of the time-dependent temperature distribution on the heater surface, which will shed light upon the effect of the porous layer on the nucleation site density and dynamics. Furthermore, if our conclusion about the effect of wettability is accurate, a lower CHF enhancement or even a CHF reduction could occur upon nanoparticle precipitation on heaters made of materials of high initial wettability. This will also have to be tested in the future.

Acknowledgments

The following sponsors are gratefully acknowledged. AREVA (PO CP04-0217), the Idaho National Laboratory (Contract no. 063, Release 18), the Nuclear Regulatory Commission (NRC-04-02-079), the DOE Innovation in Nuclear Infrastructure and Education Program (DOE-FG07-02ID14420), the Korea Science and Engineering Foundation for Mr. Kim's doctoral fellowship and the

Korea Research Foundation (KRF-2005-214-D00400) for Dr. Bang's post-doctoral fellowship.

References

[1] S. Choi, Enhancing thermal conductivity of fluids with nanoparticles, in: D.A. Siginer, H.P. Wang (Eds.), Developments and Applications of Non-Newtonian Flows, ASME, FED-Vol. 231/MD-Vol. 66, 1995, pp. 99–105.

[2] J. Buongiorno, L.-W. Hu, Nanofluid coolants for advanced nuclear power plants, Paper 5705, in: Proceedings of ICAPP'05, Seoul, 15–19 May 2005.

[3] S.M. You, J. Kim, K.H. Kim, Effect of nanoparticles on critical heat flux of water in pool boiling heat transfer, Appl. Phys. Lett. 83 (16) (2003) 3374–3376.

[4] S. Das, N. Putra, W. Roetzel, Pool boiling characteristics of nano-fluids, Int. J. Heat Mass Transfer 46 (2003) 851–862.

[5] P. Vassallo, R. Kumar, S. D'Amico, Pool boiling heat transfer experiments in silica–water nano-fluids, Int. J. Heat Mass Transfer 47 (2004) 407–411.

[6] T.N. Dinh, J.P. Thu, T.G. Theofanous, Burnout in high heat flux boiling: the hydrodynamic and physico-chemical factors, in: 42nd AIAA Aerospace Sciences Meeting and Exhibit, Reno, Nevada, 5–6 January 2004.

[7] J.H. Kim, K.H. Kim, S.M. You, Pool boiling heat transfer in saturated nanofluids, in: Proceedings of IMECE 2004, Anaheim, CA, 13–19 November 2004.

[8] G. Moreno Jr., S. Oldenburg, S.M. You, J.H. Kim, Pool boiling heat transfer of alumina–water, zinc oxide–water and alumina–water ethylene glycol nanofluids, in: Proceedings of HT2005, San Francisco, CA, USA, 17–22 July 2005.

[9] I.C. Bang, S.H. Chang, Boiling heat transfer performance and phenomena of Al_2O_3–water nano-fluids from a plain surface in a pool, Int. J. Heat Mass Transfer 48 (2005) 2407–2419.

[10] D. Milanova, R. Kumar, Role of ions in pool boiling heat transfer of pure and silica nanofluids, Appl. Phys. Lett. 87 (2005) 233107.

[11] D. Wen, Y. Ding, Experimental investigation into the pool boiling heat transfer of aqueous based γ-alumina nanofluids, J. Nanoparticle Res. 7 (2005) 265–274.

[12] H. Kim, J. Kim, M. Kim, Experimental study on the characteristics and mechanism of pool boiling CHF enhancement using nano-fluids, in: ECI International Conference on Boiling Heat Transfer, Spoleto, 7–12 May 2006.

[13] H. Kim, J. Kim, M. Kim, Experimental study on CHF characteristics of water–TiO_2 nano-fluids, Nucl. Eng. Technol. 38 (1) (2006).

[14] D. Milanova, R. Kumar, S. Kuchibhatla, S. Seal, Heat transfer behavior of oxide nanoparticles in pool boiling experiment, in: Proc. of 4th International Conference on Nanochannels, Microchannels and Minichannels, Limerick, Ireland, 19–21 June 2006.

[15] D.T. Wasan, A.D. Nikolov, Spreading of nanofluids on solids, Nature 423 (8) (2003) 156.

[16] J.G. Collier, J.R. Thome, Convective Boiling and Condensation, third ed., Oxford Science Publications, 1996.

[17] R. Cole, W. Rosenhow, Correlation of bubble departure diameters for boiling of saturated liquids, Chem. Eng. Prog. Symp. Ser. 65 (92) (1969) 211–213.

[18] R.N. Wenzel, Surface roughness and contact angle (letter), J. Phys. Coll. Chem. 53 (9) (1949) 1466.

[19] C.H. Wang, V.K. Dhir, Effect of surface wettability on active nucleation site density during pool boiling of water on a vertical surface, J. Heat Transfer 115 (1993) 659–669.

[20] S.S. Kutateladze, Heat transfer in condensation and boiling, AEC-TR-3770, 1952.

[21] N. Zuber, Hydrodynamic aspects of boiling heat transfer, AECU-4439, 1959.

[22] Y. Haramura, Y. Katto, A new hydrodynamic model of CHF applicable widely to both pool and forced convection boiling on submerged bodies in saturated liquids, Int. J. Heat Mass Transfer 26 (1983) 389–399.

[23] P. Sadasivan, P.R. Chappidi, C. Unal, R.A. Nelson, Possible mechanisms of macrolayer formation, Pool External Flow Boil. (ASME 1992) (1992) 135.

[24] Y. Katto, S. Yokoya, Principal mechanism of boiling crisis in pool boiling, Int. J. Heat Mass Transfer 11 (1968) 993–1002.

[25] T.G. Theofanous et al., The boiling crisis phenomenon. Part II: Dryout dynamics and burnout, Exp. Therm. Fluid Sci. 26 (2002) 793–810.

[26] M. Arik, A. Bar-Cohen, Effusivity-based correlation of surface property effects in pool boiling CHF of dielectric liquids, Int. J. Heat Mass Transfer 46 (2003) 3755–3764.

[27] T.G. Theofanous, T.N. Dinh, High heat flux boiling and burnout as microphysical phenomena: mounting evidence and opportunities, Multiphase Sci. Technol. 18 (1) (2006) 1–26.

[28] S.V. Gupta, Capillary action in narrow and wide tubes – a unified approach, Metrologia 41 (2004) 361–364.

[29] W. Rosenhow, P. Griffith, Correlation of maximum heat flux data for boiling of saturated liquids, Chem. Eng. Prog. Symp. Ser. 52 (18) (1956) 47–49.

[30] N. Kolev, How accurately can we predict nucleate boiling? Multi-phase Flow Dynamics, vol. 2, Springer, 2002.